The Length Dependence of Translational Diffusion, Free Solution Electrophoretic Mobility, and Electrophoretic Tether Force of Rigid Rod-Like Model Duplex DNA

Stuart Allison,* Chuanying Chen,* and Dirk Stigter†
*Department of Chemistry, Georgia State University, Atlanta, Georgia 30303, and †Department of Pharmaceutical Chemistry, University of California at San Francisco, San Francisco, California 94143 USA

ABSTRACT In this work, boundary element modeling is used to study the transport of highly charged rod-like model polyions of various length under a variety of different aqueous salt conditions. Transport properties considered include free solution electrophoretic mobility, translational diffusion, and the components of the "tether force" tensor. The model parameters are chosen to coincide with transport measurements of duplex DNA carried out under six different salt/temperature conditions. The focus of the analysis is on the length dependence of the free solution electrophoretic mobility. In a solution containing 0.04 M Tris-acetate buffer at 25°C, calculated mobilities using straight rod models show a stronger dependence on fragment length than that observed experimentally. By carrying out model studies on curved rod models, it is concluded that the "leveling off" of mobility with fragment length is due, in part at least, to the finite curvature of DNA. Experimental mobilities of long duplex DNA in monovalent alkali salts are reasonably well explained once account is taken of long-range bending and the simplifying assumptions of the model studies.

INTRODUCTION

The principal topic of the present work concerns the length dependence of the free solution electrophoretic mobilities of highly charged rigid rod models. The translational diffusion constants of the same models shall also be considered. Such structures are particularly relevant in biophysics because rods serve as realistic models for duplex DNA fragments. For example, the translational and rotational diffusion constants of short duplex DNA fragments consisting of n base pairs (bp) correspond to those of uncharged right circular cylinders of radius 1.0 nm and length $L = 0.34n$ (in nm) (Eimer et al., 1990; Nuutero et al., 1994). Theory (Tirado and Garcia de la Torre, 1979; Garcia de la Torre and Bloomfield, 1981; Tirado et al., 1984) predicts a length dependence of the translational diffusion constant, D, that varies roughly as $\ln(n)/n$. In the present study, we reconsider the translational friction/diffusion constants of rodlike models, but account for the effect of polyion and ion atmosphere charge. Physically, transport of a charged particle through a viscous medium causes the ion atmosphere around the particle to distort, and this, in turn, increases the frictional drag on the particle. This "electrolyte friction" effect has been examined theoretically (Booth, 1954; Schurr, 1980; Stigter, 1982a; Geigenmuller, 1984; Schurr, 1984; and Vizcarra-Rendon et al., 1990) and experimentally (Gorti et al., 1984) to a very limited extent.

Free solution electrophoretic mobilities of long duplex DNAs are available and the recent study by Hoagland and coworkers includes a summary of past work (Hoagland et al., 1999). Long duplex DNA mobilities are more difficult to interpret than those of short duplex DNAs due to their more complex global conformation. For DNAs substantially less than a persistence length, P, (which equals ~50 nm or ~150 bp under most salt conditions (Rizzo and Schellman, 1981)), the overall conformation can be modeled as a rigid rod. However, for fragments substantially longer than several hundred basepairs, the overall conformation is that of a random coil polymer although locally the DNA remains rodlike. Because long DNAs are locally rodlike, mobilities have been interpreted in terms of infinite rod models (Schellman and Stigter, 1977; Stigter, 1978a,b). Although this may be a good approximation for a polymer as "stiff" as duplex DNA, the influence of long-range conformation on electrophoretic mobilities is a point worth addressing, and this is done in the present work. With the development of boundary element methods that solve the coupled field equations (Allison, 1996), it is now possible to carry out electrophoretic mobility calculations on detailed model polyions such as short DNA fragment up to ~100 bp in length. Experimentally, less work has been done on short DNAs, but enough has been reported to demonstrate a rather weak dependence of mobility on length. In Tris buffers (Stellwagen et al., 1997) the free solution electrophoretic mobility displays a modest increase with length, but reaches a constant plateau value beyond ~400 base pairs.

Received for publication 22 May 2001 and in final form 30 July 2001.

Address reprint requests to Stuart Allison, Dept. of Chemistry, Georgia State University, Atlanta, GA 30303. Tel.: 404-651-1986; E-mail: chesaa@panther.gsu.edu.

0006-3495/01/11/2558/11 $2.00

METHODS

The transport properties of rigid rod structures such as those shown in Fig. 1 are determined within the framework of the continuum hydrodynamic-electrodynamic model (Overbeek, 1943; Hunter, 1981; Allison and Stigter, 2000). The solvent is represented as an incompressible Newtonian fluid with viscosity η surrounding a rigid model polyion enclosed by hydrody-

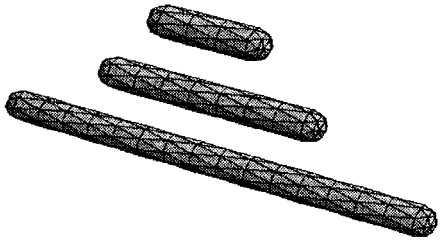

FIGURE 1 Representative straight-capped-cylinder models for 20-, 40-, and 80-bp duplex DNA. The number of plates making up these particular model structures are 112, 176, and 304, respectively.

namic shear surface S_p. The success of continuum models in accurately predicting sedimentation and diffusion constants of detailed model structures has been recognized for over twenty years (Garcia de la Torre and Bloomfield, 1981). In addition, continuum models have been very successful in treating the equilibrium electrostatics of ionic solutions. This is true for a wide range of applications from the activity of dilute solutions of simple salts (Debye–Huckel theory) to such complex problems as the ionization states of detailed model proteins (Antosiewicz et al., 1996). Under certain conditions at least, it has also been established that detailed continuum models can successfully be applied to electrokinetic transport of DNA (Allison and Mazur, 1998; Mazur et al., 2001). Recent modeling of short 18- and 20-bp DNA fragments using detailed "atomic resolution" surface models (Mazur et al., 2001) has shown that it is not necessary to include a Stern layer of solvent that moves with the polyion as a rigid body to obtain translational diffusion constants that match experiment. Experiments on other systems have shown that the solvent-accessible surface and S_p coincide to within a resolution of 1 Å (Stigter, 1982b). For the DNA systems studied in the present work, solvent-accessible surface and S_p are used interchangeably. It should be emphasized that this might not be appropriate for a deeply grooved or holed surface. However, limited studies on short DNAs (Mazur et al., 2001) suggest that the grooves have no significant effect on transport, and such effects are ignored in the present study.

The motion of the polyion is assumed small enough that the local fluid velocity at point $\mathbf{y}$, $\mathbf{v}(\mathbf{y})$, and local pressure, $p(\mathbf{y})$, are described by the linearized Navier–Stokes and solvent incompressibility equations,

$$\eta\nabla^2\mathbf{v}(\mathbf{y}) - \nabla p(\mathbf{y}) = -\mathbf{s}(\mathbf{y}), \tag{1}$$

$$\nabla\cdot\mathbf{v}(\mathbf{y}), \tag{2}$$

where $\mathbf{s}(\mathbf{y})$ is the external force per unit volume acting on the fluid at $\mathbf{y}$. For a polyion, the local charge density due to co- and counterion atmospheres, $\rho(\mathbf{y})$, interacts with the local electric field, $-\nabla\Lambda(\mathbf{y})$ (where $\Lambda(\mathbf{y})$ is the local electrostatic potential) yielding $\mathbf{s}(\mathbf{y}) = -\rho(\mathbf{y})\nabla\Lambda(\mathbf{y})$. For the transport of model structures, translational or rotational friction coefficients are determined by translating or rotating the structures with uniform linear or angular velocities through a fluid otherwise at rest. Also, "stick" boundary conditions are normally assumed in which the particle and fluid velocities match on S_p. In the present work, we are interested in the translational motion of simple model structures such as those shown in Fig. 1 where translation/rotation coupling (Happel and Brenner, 1983) can be ignored. The more general transport problem is described in detail elsewhere (Garcia Bernal and Garcia de la Torre, 1980; Garcia de la Torre et al., 1982; Mazur et al., 2001). From the solution of Eqs. 1–2 (which, in the present work, is solved numerically) it is possible to compute the force, $\mathbf{z}^{(1)}$, exerted on the fluid by the particle,

$$\mathbf{z}^{(1)} = \boldsymbol{\Xi}_t\cdot\mathbf{u}, \tag{3}$$

where $\mathbf{u}$ is the particle velocity and $\boldsymbol{\Xi}_t$ is the translational friction or resistance tensor. The (1) superscript on the force in Eq. 3 refers to case 1 transport, which means that the particle is translated through an otherwise stationary fluid with uniform velocity $\mathbf{u}$, or equivalently, the particle is held stationary and placed in a flow field where the fluid velocity far from the particle is $-\mathbf{u}$ (O'Brien and White, 1978; Allison and Tran, 1995). In case 2 transport, the particle is held stationary, but subjected to a constant external electric field, $\mathbf{e}$, and the fluid is also stationary far from the particle. The force exerted on the fluid by the particle is

$$\mathbf{z}^{(2)} = -q\mathbf{Z}\cdot\mathbf{e}, \tag{4}$$

where q is the protonic charge (4.803×10^{-10} esu) and $\mathbf{Z}$ is called the "tether force", or simply Z-tensor. In special circumstances, it is possible to fix, or tether, a large polyion in space and monitor its behavior in an external electric field (Smith and Bendich, 1990). For this reason, $\mathbf{Z}$ may be referred to as the tether force tensor. This point is discussed in more detail later. For a rodlike structure (Fig. 1) or a similar structure that is smoothly bent, it is straightforward to identify three orthogonal directions ($i = 1$ to 3) along which $\mathbf{z}^{(1)}$ is parallel to $\mathbf{u}$. In a reference frame whose axes coincide with these three orthogonal directions, $\boldsymbol{\Xi}_t$ is diagonal. The corresponding translational diffusion constant along direction i is simply

$$D_i = k_BT(\boldsymbol{\Xi}_t^{-1})_{ii}, \tag{5}$$

where k_B is Boltzmann's constant, T is absolute temperature, and the -1 superscript denotes inverse. The orientationally averaged translational diffusion constant, D, is simply the average of the three D_i (or $(D_\parallel + 2D_\perp)/3$ for a straight rod diffusing in three dimensions where $D_\parallel$ and $D_\perp$ are the diffusion constants parallel and perpendicular to the rod axis, respectively).

In general, nonequilibrium electric or flow fields distort a macromolecule's ion atmosphere from its equilibrium value (Booth, 1954; Stigter, 1982a). For a sedimenting particle (case 1 transport), this distortion or "ion relaxation" increases the frictional drag, or equivalently, reduces D_i. This electrolyte friction effect is expected to be small unless the charge on the polyion is large (Booth, 1954; Stigter, 1982a). For this reason, it is usually ignored, which is equivalent to neglecting $\mathbf{s}(\mathbf{y})$ in Eq. 1. Diffusion constants for right circular cylinder models that ignore electrolyte friction have been thoroughly studied by a number of investigators. The most comprehensive investigation is that of Garcia de la Torre and coworkers (Tirado and Garcia de la Torre, 1979; Garcia de la Torre and Bloomfield, 1981; Tirado et al., 1984) in which D_i is written

$$D_i = \frac{k_BT}{A_i\pi\eta L}(\ln p + \gamma_i), \tag{6}$$

$$\gamma_i = a_i + b_i/p + c_i/p^2, \tag{7}$$

where $A_i = 2$ ($i = 1$ (parallel to rod axis)) or 4 ($i = 2$ or 3 (perpendicular to rod axis)), L is the cylinder length, $p = L/2R$ where R is the cylinder radius, and a_i, b_i, c_i are constants tabulated elsewhere (Garcia de la Torre and Bloomfield, 1981; Tirado et al., 1984). In the remainder of the present work, p represents a reduced length ($L/2R$) rather than the pressure. The orientationally averaged diffusion constant, D, is also expressed in the same form as Eqs. 6–7 above with $A = 3$, $a = 0.312$, $b = 0.565$, $c = 0.10$ (Garcia de la Torre and Bloomfield, 1981; Tirado et al., 1984). For long rods, it is seen that the D_i (and also D) vary roughly as $\ln(n)/n$.

To include the effects of ion relaxation on diffusion, account must be taken of the external forces on the fluid near the polyion, and this requires solution ot the nonequilibrium Poisson equation

$$\nabla\cdot(\epsilon(\mathbf{y})\nabla\Lambda(\mathbf{y})) = -4\pi\rho_l(\mathbf{y}), \tag{8}$$

where $\epsilon(\mathbf{y})$ is the local dielectric constant and $\rho_l(\mathbf{y})$ is the local charge distribution. It is also necessary to solve a steady-state ion-transport equa-

tion for the local current density of each ion species $\mathbf{j}_\alpha(\mathbf{y})$

$$\nabla \cdot \mathbf{j}_\alpha = 0, \tag{9}$$

$$\mathbf{j}_\alpha = n_\alpha \mathbf{v} - D_\alpha \nabla n_\alpha + \frac{n_\alpha D_\alpha \mathbf{s}_\alpha}{k_B T}, \tag{10}$$

where n_α the local concentration of that species, $\mathbf{v}$ the fluid velocity, D_α the diffusion constant of an α ion, and $\mathbf{s}_\alpha$ the local external force on an α ion. It should be emphasized that Eqs. 1, 2, 8–10 are coupled together.

In the present work, these equations are solved by an iterative Boundary Element procedure described in detail elsewhere (Allison, 1996; Allison and Mazur, 1998; Mazur et al., 2001). Briefly, the polyion is modeled as a discrete rigid array of M plates and representative examples are shown in Fig. 1. These structures are designed to reproduce the translational diffusion constants of n-basepair duplex DNA modeled as right circular cylinders of length 0.34 n (in nm) and 1.0 nm radius (Allison and Mazur, 1998). The interior of the model is represented as a uniform low dielectric medium ($\epsilon_i = 4$) containing a line or helical charge distribution appropriate for DNA. The surrounding fluid has uniform viscosity, η, and dielectric constant, ϵ_o appropriate for water at a particular temperature. The water contains mobile ions that are treated as a continuum. The fluid domain is discretized into 49 shells that increase in thickness moving away from the polyion surface. The outermost shell is located at a distance nearest to the polyion surface of $16/\kappa$ (κ = Debye–Huckel screening parameter). Each shell, in turn, is divided into M discrete volume elements that conform closely to the polyion surface for the innermost shells. The approximation is made that physical quantities are constant on each plate on the polyion surface or each volume element in the fluid. Systematic errors inherent in this discretization approximation can be accounted for by studying a series of models in which M is varied and then extrapolating (electrophoretic mobilities, for example) to the limit $1/M \rightarrow 0$. This extrapolated shell procedure (Allison, 1999) as well as more details regarding the iterative BE procedure are described elsewhere (Allison, 1996; Allison and Mazur, 1998; Mazur et al., 2001).

In addition to case 1 transport, which is sufficient for determining friction and diffusion coefficients of model structures, it is also necessary to consider case 2 transport discussed previously in connection with Eq. 4 (stationary polyion in a constant external field, $\mathbf{e}$) when modeling electrophoretic mobility. For a weakly charged polyion in the limit of low salt, the tensor, $\mathbf{Z}$ must go to $Z_{actual}\mathbf{I}$ where Z_{actual} is the actual charge on the polyion (in protonic units) and $\mathbf{I}$ is the 3×3 identity tensor. In general, however, an external electric field will exert forces on the ion atmosphere of a polyion and this, in turn, generates hydrodynamic forces on the polyion (which is stationary in case 2 transport). Consequently, $\mathbf{Z}$, does not correspond to the total charge of the polyion, in general, and is a tensor quantity. For rodlike models, $\mathbf{Z}$ is diagonal in the same reference frame that Ξ_t is diagonal in. The diagonal components of $\mathbf{Z}$, Z_i, are determined by placing the model structure in an electric field oriented along the i-direction, computing $\mathbf{z}_i^{(2)}$ (by a numerical BE procedure), and solving Eq. 4 for Z_i. Steady-state electrophoresis can be viewed as a superposition of cases 1 and 2 such that the total force exerted by the polyion on the fluid is zero (O'Brien and White, 1978; Allison and Tran, 1995). Eqs. 3–4 are added together and the sum is set to zero. Eq. 5 is also used to introduce D_i. Define the free solution electrophoretic mobility for the model structure, $\boldsymbol{\mu}_i\mathbf{e} = \mathbf{u}$ for $\mathbf{e}$ and $\mathbf{u}$ directed along i, then

$$\mu_i = \frac{qZ_iD_i}{k_BT}. \tag{11}$$

The mobility obtained in an experiment is simply the average of the three μ_i provided the applied field is weak enough that no significant orientation of the polyion results as a consequence of the applied field. These conditions are readily achieved in actual experiments (Stellwagen et al., 1997).

Characterizing the Z_i and μ_i length dependencies

As discussed previously, the D_i decrease with length roughly as $\ln(n)/n$ or $\ln(L)/L$ and deviations from this overall behavior are contained in the correction terms, γ_i (Eq. 6), which are themselves length dependent. What are convenient representations for Z_i and μ_i? Experimentally, the (orientationally averaged) electrophoretic mobility of duplex DNA exhibits a weak length dependence relative to diffusion and appears to reach a constant plateau value above several hundred basepairs (Stellwagen et al., 1997). In view of Eq. 11 and the known dependence of D_i on length, we can expect the length dependence of Z_i to vary approximately as $n/\ln(n)$ (or equivalently $n/\ln(p)$). A simple functional definition which exhibits this general characteristic is

$$X_i = -2n/Z_i = d_i\ln(p) + e_i. \tag{12}$$

In the limit of long DNA, only the d_i term remains. The coefficients d_i and e_i (assumed constant in the present work) are determined by fitting the length dependence of the $\mathbf{Z}$, or tether force tensor components.

Once the coefficients for γ_i and X_i are known, it is straightforward to construct simple equations for the length dependence of parallel and perpendicular mobilities. Combining Eqs. (5, 6, 11, and 12)

$$\mu_\parallel = -\alpha\left[\frac{\ln(p) + \gamma_\parallel}{d_\parallel\ln(p) + e_\parallel}\right], \tag{13}$$

$$\mu_\perp = -\frac{\alpha}{2}\left[\frac{\ln(p) + \gamma_\perp}{d_\perp\ln(p) + e_\perp}\right] \tag{14}$$

where $\alpha = q/\pi\eta h$ and $h = 0.34$ nm is the rise per basepair of duplex DNA. At 20°C in water, $\eta = 1.002$ cp and (making use of the conversion factor 1 esu = 300 V cm) $\alpha = 1.499 \times 10^{-3}$ cm^2/V sec. Some caution should be exercised in applying these equations to very short or very long fragments because the parameters are determined by fitting data from fragments in the size range of 20–100 bp. For this size range, $\ln(p)$ varies from 1.224 (20 bp) to 2.833 (100 bp) and Eqs. 13 and 14 should not be used far outside of these ranges.

We are also interested in dimensionless mobilities defined by

$$C_i = \frac{4\pi\eta q}{\epsilon_o k_B T}\frac{\mu_i}{y_S}, \tag{15}$$

where

$$y_S = \frac{q\langle\Lambda_0\rangle_S}{k_BT}, \tag{16}$$

and $\langle\Lambda_0\rangle_S$ is the equilibrium electrostatic potential averaged over the polyion surface. For thin double-layer polyions (those whose smallest linear dimensions are large relative to $1/\kappa$) in the absence of ion relaxation, C_i equals 1 (Smoluchowski, 1921). For thick double-layer spherical polyions of uniform surface potential in the absence of ion relaxation, C_i equals ⅔ (Huckel, 1924; Henry, 1931). In general, ion relaxation always reduces C_i relative to the no-ion relaxation limit. To characterize the length dependence of the C_i, the following fitting polynomial is used

$$C_i = f_i(1 + g_i/p + h_i/p^2). \tag{17}$$

Conditions for the Length Studies

A transport property of a particular (highly charged) model particle depends in a complex way on temperature, T, solvent viscosity, η, polyion and solvent dielectric constants, (ϵ_i and ϵ_0, respectively), salt concentration, c_0 (assumed monovalent in the present work), and the mobility or diffusion constants, D_α, of the particular small-ion species present. This can be

readily understood by considering the various coupled continuum equations that must be solved. One simplifying feature is that mobility appears to be nearly independent of the assumed dielectric constant within the polyion, ϵ_i, and this quantity is set to 4 (Mazur et al., 2001). Experimental measurements of the free solution mobility of DNA have been have been carried out under a wide variety of conditions, and, because of that, it will be necessary to carry out length studies under different temperature, ionic strength, and ion-type conditions as well. An additional complicating feature involves specific interactions between small ions and DNA that go beyond the purely electrostatic interactions present in current modeling. There remains little doubt that such interactions occur as the different mobilities of DNA in Tris-acetate and Tris-borate buffers under otherwise identical experimental conditions demonstrate (Stellwagen et al., 1997, 2000). With regard to past modeling, it should be mentioned that the electrophoretic mobility of 20-bp DNA in 0.11 M KCl at 20°C measured by the technique of membrane-confined analytical electrophoresis (Laue et al., 1996) are fairly well explained by continuum modeling. The model mobilities are ~4–6% higher than experiment under these conditions (Allison and Mazur, 1998; Mazur et al., 2001). In contrast, the electrophoretic mobility of 18-bp DNA in 0.04 M Tris-acetate buffer (pH = 8) at 25°C measured by capillary electrophoresis (Stellwagen et al., 1999) has been more difficult to model. Continuum modeling under these conditions yields mobilities that are ~28% higher than experiment (Mazur et al., 2001). Our interpretation is that there is an attractive interaction, possibly hydrogen bonding, between $Tris^+$ and DNA, in addition to electrostatic interaction, that is not accounted for in our continuum modeling. In fact, reducing the phosphate charges of DNA by ~50%, or equivalently "binding" half of the anionic phosphates with $Tris^+$ cations yields mobilities in good agreement with experiment. There may also be additional interactions between alkali ions such as K^+ and DNA, but the mobility data mentioned above argues that such interactions would be significantly weaker than for $Tris^+$. In the present study, length studies are limited to six cases that cover some of the key experimental conditions used.

The most thorough study of the length dependence of duplex DNA mobilities is the work of Stellwagen et al. (1997). Their experiments were carried out in water at 25°C (η = 0.89 cp, ϵ_0 = 78.3) in a buffer consisting of 0.04 M Tris-acetate plus 1 mM EDTA. The buffer was prepared by titrating Tris base with acetic acid until pH = 8. A buffer prepared in this way contains 0.02 M $Tris^+$ and $acetate^-$. From limiting molar conductivities of $Tris^+$ (Klein and Bates, 1980) and $acetate^-$ (CRC Handbook of Chemistry and Physics), hydrodynamic radii of 0.3136 and 0.2278 nm can be assigned to the ions (Mazur et al., 2001). As discussed before, a model with the charges of the DNA reduced by 50% gives the best agreement with experiment. Because capped cylinder models yield mobilities in excellent agreement with more realistic surface models for short fragments (Mazur et al., 2001), all models considered in the present work are of the simpler capped-cylinder variety. In addition, the charge distribution within the DNA models are usually approximated with a simple line-charge distribution. However, the effects of replacing the line-charge distribution with a more realistic double-helical one and including curvature in the rod models will be considered briefly. All studies in 0.02 M $Tris^+$ $acetate^-$ at 25°C with DNA phosphates set to half their full charge are called condition I.

All remaining conditions will have the DNA phosphates fully charged and, unless otherwise stated, the polyion charge is represented as a line of charges and the cylinder models are straight. Conditions II–V are in water at 20°C (η = 1.002 cp, ϵ_0 = 80.36). Condition II is in 0.02 M $Tris^+$ $acetate^-$, condition III in 0.02 M NaCl, condition IV in 0.02 M KCl, and condition V in 0.11 M KCl. The hydrodynamic radii of Na^+, K^+, and Cl^- are set equal to 0.1837, 0.1242, and 0.1242 nm, respectively, on the basis of their limiting molar conductivities (CRC Handbook of Chemistry and Physics). Condition III is chosen to make contact with recent capillary electrophoresis studies of Hoagland et al. (1999) on long duplex DNA. The membrane-confined capillary electrophoresis studies of Laue et al. (1996) on short DNAs were carried out under conditions very similar to condition V. Conditions II–V also provide insight into the effect of small-ion mobility and ionic strength on transport properties of DNA models. Finally, condition VI is carried out in 0.2 M KCl at 1.3°C (η = 1.711 cp, ϵ_0 = 87.49). This reproduces one of the experimental conditions used in a widely cited early study on the mobility of long DNA (Ross and Scruggs, 1964). The key variables used in the model studies for the six conditions are summarized in Table 1.

TABLE 1 Conditions for length studies

Condition	Charge Model	T (°C)	c_0 (M)	Salt Type
I	half charge	25	0.02	$Tris^+$ $Acetate^-$
II	full charge	20	0.02	$Tris^+$ $Acetate^-$
III	full charge	20	0.02	NaCl
IV	full charge	20	0.02	KCl
V	full charge	20	0.11	KCl
VI	full charge	1.3	0.20	KCl

Electrolyte friction

As discussed previously, ion relaxation of highly charged polyions is expected to reduce the parallel and perpendicular components of the translational diffusion tensor of a straight rod model structure ($D_\parallel$ and $D_\perp$, respectively) and the orientationally averaged translational diffusion constant, D, relative to that of an uncharged model. Because this electrolyte friction effect is readily obtained in the course of determining electrophoretic mobilities from model structures, results are presented in an abbreviated form. A detailed treatment will be postponed to a later date when experimental data on DNA fragments becomes available. To explore the effects of additional frictional drag due to ion relaxation, define

$$\Delta_i = \frac{1}{D_i(r)} - \frac{1}{D_i(nr)}, \tag{18}$$

where i refers to parallel or perpendicular orientations, and r and nr to ion relaxation included and not included, respectively. Considering Eqs. 3 and 5, it can be seen that Δ_i is proportional to the additional frictional drag ion relaxation generates on a model rodlike polyion in a particular orientation. Figure 2 shows the length dependence of $\Delta_\parallel$ and $\Delta_\perp$ for fully charged DNA rod models in 0.11 M KCl at 20°C (condition V). In the length studies for diffusion and electrophoresis, six models are examined corresponding to 20, 30, 40, 60, 80, and 100 bp. The number of plates in the structures usually ranges from 112 (20 bp) to 368 (100 bp), but for certain fragment lengths, much more extensive studies are made over a wide range of plate numbers to make the extrapolated shell corrections (Allison, 1999). For the perpendicular orientation, $\Delta_\perp$ exhibits a nearly linear variation with rod length or number of base pairs, n. Consider a long rod translating perpendicular to its long axis. Ion relaxation results in a perturbed dipolar charge

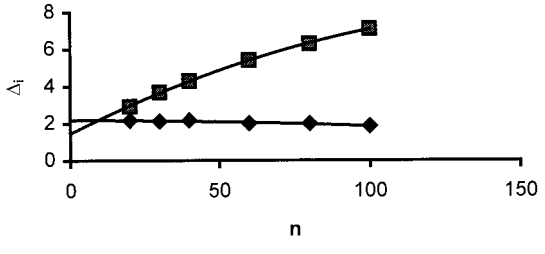

FIGURE 2 Δ_i versus n. Diamonds correspond to parallel and squares to perpendicular difference components. The model conditions are condition V (full charge DNA, 0.11 M KCl, 20°C).

TABLE 2 Electrolyte friction effect versus length under different conditions (100 (1 − $D(r)/D(nr)$))

	$n=$					
Condition	20	30	40	60	80	100
I	7.21	7.32	7.14	6.57	6.06	5.63
II	12.62	12.01	11.43	10.10	9.15	8.48
III	8.46	8.24	7.76	6.88	6.19	5.70
IV	6.48	6.17	5.94	5.23	4.75	4.41
V	2.78	2.66	2.47	2.12	1.92	1.75
VI	1.86	1.73	1.60	1.42	1.29	1.23

distribution that is essentially constant with position along the rod except at the ends (Stigter, 1978b, Allison et al., 1999). Hence, the additional frictional drag required to maintain that perturbed charge distribution should vary linearly with length. For a long rod translating parallel to its axis, the perturbed charge densities nearly vanish, except at the ends of the rod (Allison, et al., 1999). If we make the reasonable assumption that the perturbed charge densities at the rod ends are independent of rod length, then the frictional drag force required to maintain that charge distribution should be independent of length. Figure 2 is consistent with this simple physical picture.

Table 2 summarizes the fractional decrease in orientationally averaged translational diffusion constants due to ion relaxation as a function of length (n = 20–100 bp) for the six conditions discussed previously. Under the conditions considered, the electrolyte friction effect is predicted to be approximately 10% or less. Increasing the polyion linear charge density, reducing the length of the polyion, or reducing the salt concentration increases the effect. Also, the effect varies inversely with the mobility of the small ions (comparing conditions II–IV).

To put the electrolyte friction effect on a more quantitative footing, the basic mathematical form for the diffusion constants of rodlike polyions, Eqs. 6–7, are retained, but the correction polynomials, $\gamma_{\|}$, $\gamma_{\perp}$, and γ, are determined with the inclusion of ion relaxation. As discussed elsewhere (Allison and Mazur, 1998), the rod models themselves are designed to reproduce Eqs. 6–7 when ion relaxation is not included (Garcia de la Torre and Bloomfield, 1981; Tirado et al. 1984), so deviations in the polynomial coefficients of Eq. 7 from the no ion relaxation values reflects the influence of ion relaxation. These polynomial coefficients are summarized in Table 3 for the six conditions discussed previously. Figure 3 shows the behavior of γ (*diamonds*, no ion relaxation; *squares*, ion relaxation) versus length for condition V, and the solid lines through the data points represent the polynomial fits.

AVERAGE SURFACE POTENTIAL AND TETHER FORCE TENSOR

Equilibrium electrostatic potentials of infinitely long (Stigter, 1975) and finite (Allison, 1994) rod models in the framework of the nonlinear Poisson–Boltzmann equation have been available for some time. The reduced surface potential averaged over the polyion surface, y_S (see Eq. 16), is computed at the start of a boundary element (BE) modeling study, and its value for the different lengths under the six conditions studied in this work are summarized in Table 4. At equilibrium, conditions II–IV are equivalent because the ion size enters the model only through their diffusion constants, D_α, appearing in Eq. 10. These exhibit roughly a linear dependence on $1/L$ or $1/p$ ($p = L/2R$ where L is the rod length and R the radius). The infinite rod, or $1/p \rightarrow 0$

TABLE 3 Polynomial coefficients for $\gamma_{\|}$, $\gamma_{\perp}$, and γ

Condition	Orientation	a_i	b_i	c_i
nr*	∥	−0.207	0.980	−0.133
nr*	⊥	0.839	0.185	0.233
nr*	ave†	0.312	0.565	0.100
I	∥	−0.316	0.594	1.341
I	⊥	0.560	0.753	−0.328
I	ave†	0.122	0.674	0.514
II	∥	−0.411	0.517	1.743
II	⊥	0.488	0.481	0.270
II	ave†	0.038	0.508	0.982
III	∥	−0.330	0.562	1.39
III	⊥	0.579	0.370	0.435
III	ave†	0.124	0.470	0.904
IV	∥	−0.304	0.702	0.943
IV	⊥	0.640	0.383	0.211
IV	ave†	0.168	0.552	0.548
V	∥	−0.238	0.948	0.058
V	⊥	0.750	0.106	0.626
V	ave†	0.258	0.487	0.437
VI	∥	−0.228	0.098	−0.010
VI	⊥	0.769	0.167	0.402
VI	ave†	0.271	0.567	0.206

*nr, no relaxation values (Tirado et al., 1984).
†ave, polynomial fit of orientationally averaged γ.

limit is given in the far right column of Table 4. Although there is considerable variation in y_S, depending on conditions, more uniformity is observed if y_S is divided by the infinite rod limit under the appropriate conditions, y_∞. This is illustrated in Fig. 4, where w is defined as y_S/y_∞. The near linear behavior of y_S or w with $1/p$ is consistent with a simple two-state model in which the local surface potential is y_{end} near the ends of the rod and y_∞ in the interior. Let λ

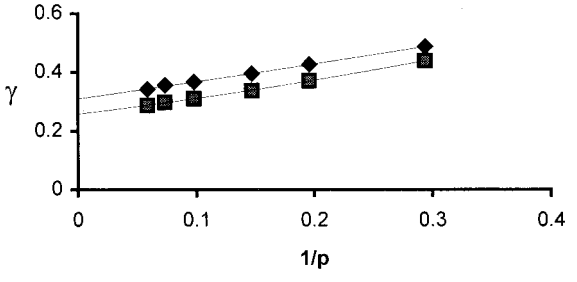

FIGURE 3 γ versus $1/p$. The correction polynomial, γ, (Eqs. 6 and 7) for translational diffusion in the absence (*diamonds*) and presence (*squares*) of ion relaxation. Solid lines represent quadratic fits.

TABLE 4 $-y_S$ Versus length under different conditions

	$n=$						
	20	30	40	60	80	100	∞
$-y_S$(I)	3.256	3.415	3.513	3.612	3.656	3.670	3.782
$-y_S$(II–IV)	4.952	5.084	5.176	5.287	5.306	5.323	5.426
$-y_S$(V)	3.486	3.578	3.664	3.731	3.753	3.770	3.845
$-y_S$(VI)	2.972	3.066	3.133	3.202	3.218	3.226	3.300

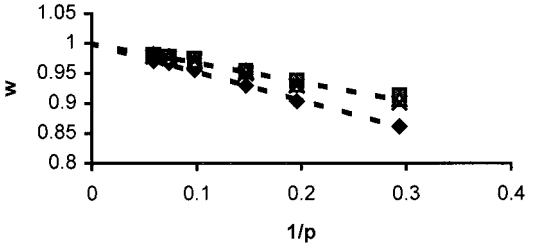

FIGURE 4 Variation in average surface potential with length. Diamonds, condition I; *filled squares*, conditions II–IV; *triangles*, condition V; and ×, condition VI.

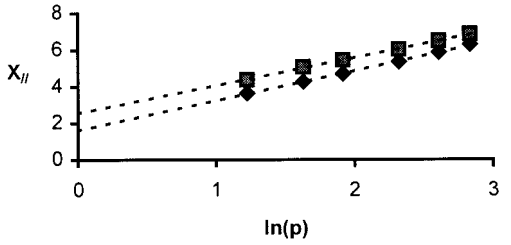

FIGURE 5 Variation in $X_{\|}$ with length. Triangles correspond to the case without ion relaxation and diamonds to the case with ion relaxation. The model conditions are condition V (full charge DNA, 0.11 M KCl, 20°C).

denote the distance from the ends of the rod where the surface potential is best described by y_{end}. The fraction of the rod surface where the reduced surface potential is y_{end} is then $2\lambda/L$, and the fraction of the rod surface where the reduced surface potential is y_∞ is $1 - 2\lambda/L$. Thus, the overall average reduced surface potential can be written as

$$y_S = y_\infty - \frac{2\lambda}{L}(y_\infty - y_{end}), \tag{19}$$

or equivalently,

$$w = 1 - \frac{2\lambda}{L}\left(1 - \frac{y_{end}}{y_\infty}\right). \tag{20}$$

The data in Table 4 and Fig. 4 exhibit the length dependence predicted by the simple two-state model described above. At first glance, it might appear unusual that the slopes of w versus $1/p$ are similar for cases II–VI (full-charge DNA models) despite the wide range of solvent conditions. However, the counterion concentration near the surface of uniform, highly charged polyions is nearly independent of the bulk ion concentrations (Rouzina and Bloomfield, 1996). Thus, we would expect λ to be independent of solvent/buffer conditions for a particular charge model and hence the slope of w versus $1/p$ similar for conditions II–VI.

Attention is now turned to the tether force tensor, **Z**. In a reference frame whose axes correspond to the principal axes of the rod, **Z** will be diagonal. However, the components parallel, $Z_{\|}$, and perpendicular, $Z_\perp$, to the rod axis will be different, in general. As discussed previously, these components cannot be equated to the bare polyion charge, or the electrophoretic charge, which is the bare charge of the polyion itself plus any ions trapped within the hydrodynamic shear surface (Schellman and Stigter, 1977; Stigter, 2000). Also, it is not a thermodynamic charge such as that extracted from the preferential interaction coefficient determined in equilibrium dialysis experiments (Olmstead et al., 1989), because it depends on such nonequilibrium quantities as the solvent viscosity and small-ion diffusion constants or mobilities. The closest direct experimental measurement of **Z** comes from electrophoretic stretch experiments on high molecular-weight circular plasmid DNAs that are held, or tethered, in place by agarose fibers threaded through their centers (Smith and Bendich, 1990). Theories have been developed to explain electrophoretic stretch (Schurr and Smith, 1990; Stigter, 1991; Stigter and Bustamante, 1998), and the electrophoretic force of Stigter and Bustamante is equivalent to $\mathbf{z}^{(2)}$ in the present work. Provided that its precise definition is kept in mind, the tether force tensor, **Z**, should be a useful transport property in the same sense as the translational friction tensor, Ξ_t.

Following procedures similar to those described previously for friction/diffusion, we consider fits to X_i defined by Eq. 12 or fits to the orientationally averaged $X = -2n/Z$, where $Z = (Z_{\|} + 2Z_\perp)/3$. Figures 5, 6, and 7 show the length dependence and linear fits (see Eq. 12) to $X_{\|}$, $X_\perp$, and X, respectively for condition V (full charge DNA, 0.11M KCl at 20°C). Diamonds correspond to the case of no ion relaxation and squares to the case with ion relaxation. Dotted lines represent linear fits to the simple functional form of Eq. 12. One could interpret $1/X$ as an absolute effective charge per base pair of DNA. (For reasons discussed elsewhere, however, that terminology is discouraged (Stigter, 2000)). From Fig. 7, it is clear that there is a pronounced length dependence of $1/X$, and this behavior is seen under all of the conditions studied in this work. The longer the DNA, the lower the absolute effective charge per base pair, and the higher the fraction of associated counterions. This trend is qualitatively consistent with equilibrium effective charges extracted from preferential interaction coefficients (Olmstead et al., 1989). The Case 2 transport coefficients defined by Eq. 12 for all six conditions are summarized in Table 5.

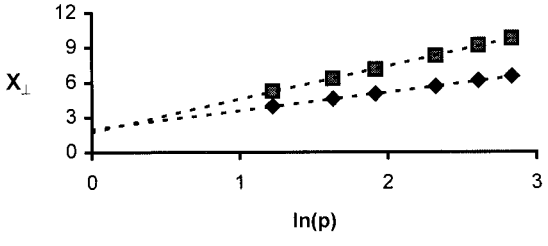

FIGURE 6 Variation in $X_\perp$ with length. Triangles correspond to the case without ion relaxation and diamonds to the case with ion relaxation. The model conditions are condition V (full charge DNA, 0.11 M KCl, 20°C).

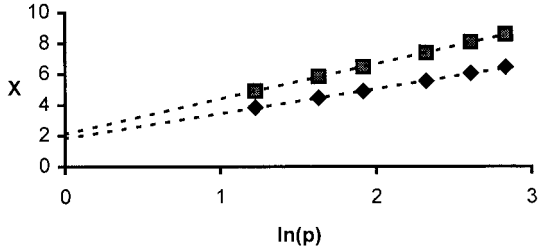

FIGURE 7 Variation in X with length. Triangles correspond to the case without ion relaxation and diamonds to the case with ion relaxation. The model conditions are condition V (full charge DNA, 0.11 M KCl, 20°C).

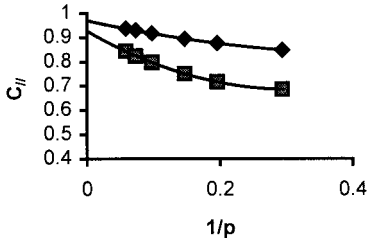

FIGURE 8 Variation in $C_{\|}$ with length. Triangles correspond to the case without ion relaxation and diamonds to the case with ion relaxation. The model conditions are condition IV (full charge DNA, 0.11 M KCl, 20°C).

With the data contained in Tables 3 and 5, Eqs. 13 and 14 can be used to estimate the electrophoretic mobility for the six conditions considered for rod models of any length. We shall return to this point later.

REDUCED MOBILITIES

Rather than fitting the model mobilities directly, we instead fit the reduced mobilities defined by Eq. 15. The length dependence of actual mobilities and a comparison of model and experimental values is given in the next section. Ion relaxation affects the parallel and perpendicular mobilities differently, and these differences depend on length. Consider first the parallel component for condition V (full charge DNA, 0.11 M KCl at 20°C) where $C_{\|}(nr)$ (*upper curve*) and $C_{\|}(r)$ (*lower curve*) versus length are plotted in Fig. 8. $C_{\|}(nr)$ varies gradually with $1/p$ and extrapolates to a value of 0.970 in the limit $1/p \rightarrow 0$. This is in fairly good agreement with the Smoluchowski value of 1.00 expected for a polyion of uniform surface potential whose linear dimensions are large compared to the thickness of the ionic double layer (Smoluchowski, 1921). To a good approximation, $C_{\|}(r)$ approaches the no ion relaxation limit as $1/p \rightarrow 0$ as postulated previously (Stigter, 1978b). The solid curves in Fig. 8 represent quadratic fits to the six models studied ranging from 20 to 100 bp. The fact that $C_{\|}(r)$ and $C_{\|}(nr)$ do not extrapolate to precisely the same value as $1/p \rightarrow 0$ is a consequence of the small number of lengths considered and the functional form of the fitting polynomial. If, for example, the data is fit as a quadratic function of $1/\ln(p)$ rather than $1/p$, then $C_{\|}(nr)$ extrapolates to 1.06 and $C_{\|}(r)$ extrapolates to 1.17 as $1/\ln(p) \rightarrow 0$. Additional modeling studies on longer rods would provide more accurate estimates of the long-rod behavior of both $C_{\|}(nr)$ and $C_{\|}(r)$, but such studies are not really necessary and would be costly. The equivalence of $C_{\|}(nr)$ and $C_{\|}(r)$ in the long-rod limit can be readily understood on physical grounds because ion relaxation for a long-rod polyion undergoing steady-state electrophoresis parallel to the rod axis will be confined to the rod ends (Stigter, 1978b; Allison et al., 1999). Thus, the reduction in parallel mobility due to ion relaxation should go to zero for sufficiently long rods, and that trend is seen at least qualitatively in Fig. 8.

TABLE 5 Tether force tensor coefficients: d_i and e_i (Ion relaxation included)

Condition	Orientation	d_i	e_i
I	∥	1.676	2.841
I	⊥	3.121	1.550
I	ave	2.506	2.153
II	∥	1.282	2.326
II	⊥	2.906	0.547
II	ave	2.196	1.374
III	∥	1.262	2.161
III	⊥	2.667	0.717
III	ave	2.057	1.389
IV	∥	1.176	2.250
IV	⊥	2.624	0.735
IV	ave	1.964	1.462
V	∥	1.519	2.541
V	⊥	2.857	1.695
V	ave	2.273	2.125
VI	∥	1.782	2.536
VI	⊥	2.782	2.114
VI	ave	2.370	2.326

Very different behavior is seen for the "without relaxation" (*top curve*) and "with relaxation" (*lower curve*) perpendicular components in Fig. 9. $C_{\perp}(nr)$ and $C_{\perp}(r)$ do not extrapolate to the same value as $1/p \rightarrow 0$. In this case, ion relaxation is not confined to the rod ends, but occurs over the entire length of the rod (Stigter, 1978a). On average, all orientations will be sampled in an experiment and we can conclude that ion relaxation reduces the average mobility of

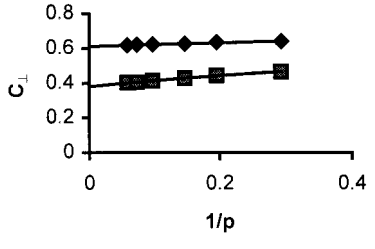

FIGURE 9 Variation in $C_{\perp}$ with length. Triangles correspond to the case without ion relaxation and diamonds to the case with ion relaxation. The model conditions are condition IV (full charge DNA, 0.11 M KCl, 20°C).

TABLE 6 Reduced mobility polynomial coefficients: f_i, g_i, and h_i (Ion relaxation included)

Condition	Orientation	f_i	g_i	h_i
I	∥	0.864	−2.065	4.048
I	⊥	0.349	1.387	−0.734
I	ave	0.520	−0.521	1.906
II	∥	0.760	−2.803	5.546
II	⊥	0.271	1.672	−1.126
II	ave	0.434	−0.938	2.763
III	∥	0.806	−2.584	5.191
III	⊥	0.298	1.530	−0.976
III	ave	0.467	−0.831	2.559
IV	∥	0.836	−2.554	4.976
IV	⊥	0.312	1.471	−0.910
IV	ave	0.487	−0.838	2.472
V	∥	0.928	−1.716	2.819
V	⊥	0.380	0.966	−0.700
V	ave	0.563	−0.501	1.224
VI	∥	0.939	−1.306	1.958
VI	⊥	0.435	0.508	0.198
VI	ave	0.603	−0.431	1.104

rodlike polyions no matter how long they are, although the effect is expected to be more significant for short rods than for long ones. The polynomial coefficients for the C_i under the six conditions considered in this paper are summarized in Table 6. For the sake of brevity, only the cases with ion relaxation are included.

COMPARISON WITH EXPERIMENT

Measurements of the free solution electrophoretic mobility of 27-bp and longer duplex DNA fragments (Stellwagen et al., 1997) were carried out in 0.04 M Tris-acetate aqueous buffer at 25°C and pH = 8.0. More recently, the same workers reported the mobility of an 18-bp duplex DNA under the same conditions (Stellwagen et al., 1999). Detailed modeling of the 18-bp fragment (Mazur et al., 2001) led us to conclude that a charge model of DNA in which the bare phosphate charges are reduced by 50% reproduced the experimental mobility quite well. Physically, this corresponds to a net charge of about +18 (neutralization of half of the DNA phosphates) from the $Tris^+$ cations being bound or entrapped within the hydrodynamic shear surface of the DNA. Thus, we expect the condition I modeling results to be the most appropriate to use in a comparison with the experimental results. The diamonds in Fig. 10 correspond to the condition I model mobilities and the solid line is a fitting curve through these points. The dashed line at $\mu = 4.24$ (in -10^{-4} cm^2/V s) is an independent model mobility for an infinitely long cylinder using the same polyion radius/linear charge density and solvent conditions used in the BE modeling studies (Stigter, 1978a,b). The underlying methodology used by Stigter and the present BE modeling studies is essentially the same, so the mobilities should agree in the limit of very long rods, and this is confirmed by Fig. 10. The

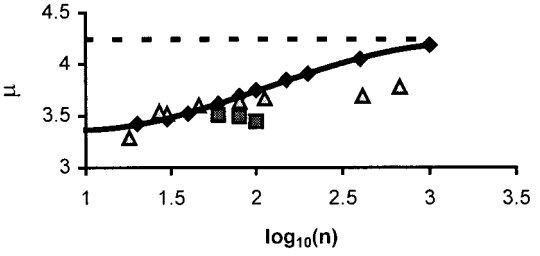

FIGURE 10 Length dependence of μ. Comparison of theory and experiment. *Diamonds* and *solid curve*, condition I modeling for straight rods; *squares*, condition I modeling for bent rods; *triangles*, experiments (Stellwagen et al., 1997). The dashed line is the model mobility of an infinitely long straight rod (Stigter, 1978a,b) under the same conditions as the BE modeling.

triangles represent experimental mobilities (Stellwagen et al., 1997, 1999). Up to ~60 bp, model and experimental mobilities are in good agreement with each other. However, the model mobilities do not appear to level off with increasing length to the extent seen in experiment. This trend is also seen under the other conditions modeled.

A possible explanation could be that bending of DNA is responsible for the leveling off of μ for long fragments. The persistence length, P, of DNA is approximately 50 nm, or 147 bp, though this value exhibits some variation with salt concentration (Rizzo and Schellman, 1981). Thus, for DNA shorter than, say, $P/2$ (approximately 80 bp), a straight rod model would be expected to be a realistic representation of the fragment. For longer DNAs, a model that accounts for bending would be more realistic. One approach would be to generate an ensemble (100, for example) of different wormlike chain conformations, model the μ of each, and average the results (Hagerman and Zimm, 1981). Unfortunately, this is not feasible due to the long simulation times involved. Computation time varies roughly as the square of the number of plates comprising the structure, and, for a 240-plate straight rod model (typical of 60-bp DNA), a complete calculation of diffusion and electrophoretic mobility with ion relaxation requires approximately two days of single processor time on a Silicon Graphics 4D-380-SX computer. A simpler approach is to generate a single bowed structure that reflects the curvature expected in an actual DNA fragment and compute the mobility for that structure, and that is the procedure followed in the present work. For a wormlike chain, the mean square end-to-end distance, $\langle R^2 \rangle$, is related to contour length, L, and persistence length by the relation (Hagerman and Zimm, 1981, or most texts relevant to polymer theory),

$$\langle R^2 \rangle = 2PL\left(1 - \frac{P}{L}\left(1 - e^{-L/P}\right)\right). \qquad (21)$$

A single bent structure is generated with sufficient curvature to yield the same $\langle R^2 \rangle$ as predicted by Eq. 21. Two capped cylinder models appropriate for 100-bp DNA are shown in

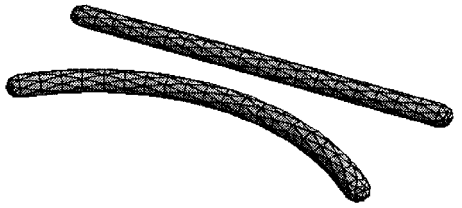

FIGURE 11 Straight and bent rod capped-cylinder models for 100-bp DNA. The bent structure has the same mean-square end-to-end distance as a wormlike chain of contour length = 34 nm and persistence length = 50 nm.

Fig. 11. The upper figure is a straight rod model and the lower a bent rod with a radius of curvature that gives the same $\langle R^2 \rangle$ as a wormlike chain with $P = 50$ nm and $L = 34$ nm. Boundary element modeling is then carried out on the bent structure, but it is necessary to consider case 1 and case 2 transport along three orthogonal directions. The filled squares in Fig. 10 represent the extrapolated shell mobilities of bent cylinder models corresponding to $P = 50$ nm for 60-, 80-, and 100-bp DNAs. These results show that the model mobilities do indeed level off and actually start to decrease. Actual duplex DNAs are not smoothly bending rods such as the bent rod models considered here. Nonetheless, these results do show that rod curvature causes μ to be slightly lower than for the corresponding straight rod. Thus, we conclude that the leveling off of μ for long fragments may be attributed, in part, to bending of the DNA.

The effects of global conformation on mobility have also been examined for condition III (0.02 M NaCl at 20°C, full charge model). For straight rods, the orientationally averaged mobilities in the presence of ion relaxation, $\mu(r)$ (in -10^{-4} cm^2/V s), are 4.01, 4.13, 4.22, and 4.32 for 40, 60, 80, and 100 bp, respectively. These are substantially higher than the value of 3.84 inferred from Fig. 11 of Hoagland et al. (1999) for high molecular-weight DNA under the same conditions. However, the bent rod ($P = 50$ nm) model mobilities for 60, 80, and 100 bp are 4.05, 4.00, and 3.89, respectively. As in the condition I studies considered previously, accounting for DNA bending in the approximate manner of the present work helps to reconcile theory and experiment with regards to the mobilities on long duplex DNA. However, without mobility experiments as a function of length similar to those of Stellwagen et al. (1997), but under different salt/buffer conditions, it is difficult to quantify the effect of bending on length. If we assume the leveling off in μ with length is similar for the six conditions studied in this work, then model mobilities corresponding to 40–60 bp should be more appropriate to compare with experimental mobilities than with model mobilities from very long rods. In 0.02 M NaCl at 20°C and fully charged, straight rod DNA models, the 40- and 60-bp $\mu(r)$ are 4.4 and 7.6% higher than the experimental value of 3.84 (Hoagland et al., 1999). In 0.2 M KCl at 1.3°C (condition VI), model mobilities for 40- and 60-bp DNA fragments are 1.96 and 2.00 for 40 and 60 bp. These are 6.5 and 8.7% higher than the experimental mobility of 1.84 (Ross and Scruggs, 1964). Also in KCl, but at a concentration of 0.11 M and at 20°C, a detailed analysis of 20-bp DNA gave a capped-cylinder, model mobility that was larger than experiment by 5.5% (Mazur et al., 2001). In this case, the charge model was a full charge model, but the charges were distributed on a double-helical spiral rather than on a line at the center of the rod axis. A more realistic helical charge distribution reduces the mobility (Allison and Mazur, 1998), but the effect is small and amounts to 1–2%. Also, going to a more realistic surface model reduces mobilities slightly, but again the reduction is in the 1–2% range. The experimental mobilities of long duplex DNA in monovalent alkali salts (Ross and Scruggs, 1964; Hoagland et al., 1999) are reasonably well explained by the model studies once account is taken of the long-range bending of high molecular-weight DNA and the simplifying assumptions of the model studies (line charge, smooth cylinder surface model of polyion).

SUMMARY

The primary motivation of the present work is the extension of BE modeling studies of the free solution electrophoretic mobility of short DNA fragments to the long fragment regime. It is concluded that long-range bending of DNA makes a small but significant contribution to mobility, and that, accounting for it, helps to reconcile theoretical mobilities on long rods (Stigter, 1978a,b) with experiment (Ross and Scruggs, 1964; Stellwagen et al., 1997; Hoagland, et al., 1999, and references cited therein). Our earlier conclusion that the mobility of short DNA can be fairly well explained by models in which there is little alkali metal counterion entrapment within the Stern layer also appears to hold when the analysis is extended to long DNAs. Because calculated mobilities tend exceed experimental mobilities by a few percent in these cases, some entrapment of alkali metal ions may be occurring. When the counterion is $Tris^+$, however, substantial entrapment is involved. It should be pointed out that $Tris^+$ contains three OH groups capable of forming hydrogen bonds with DNA, and hydrogen bond formation is likely to be the cause of the entrapment of the $Tris^+$ counterions. In the BE modeling, account is taken of the purely electrostatic interactions between counterion and the charges within the polyion itself, but no additional interactions (such as H-bond interactions) are accounted for. The early work of Ross and Scruggs (1964) also included a study of tetramethylammonium ions, TMA^+, which appear to interact less strongly with DNA than simple alkali counterions. In this case, the bulky nature of the counterion gives rise to excluded volume interactions that produce an effect on the mobility just the opposite of $Tris^+$.

The most straightforward applications of BE modeling to electrokinetic transport is to free solution electrophoresis (Laue et al., 1996; Stellwagen et al., 1997; Rasmusson and Akerman, 1998; Hoagland et al., 1999) and its application to DNA of moderate length has been described in the present work. Its extension to the very useful technique of gel electrophoresis (Calladine et al., 1991; Gurrieri et al., 1999) is currently underway. In addition to electrophoresis, the BE methodology should be of value in interpreting the primary electroviscous effect (Sherwood, 1980; Allison, 1998) of highly charged particles and macromolecules including dilute solutions of DNA, silica sols (Biddle et al., 1996), and linear polyelectrolytes such as poly(styrenesulfonate) (Jiang et al., 2001).

We would like to acknowledge National Science Foundation Grant MCB-9807541 for partial support of this work.

REFERENCES

Allison, S. A. 1994. End effects in electrostatic potentials of cylinders: models for DNA fragments. *J. Phys. Chem.* 98:12091–12096.

Allison, S. A. 1996. Modeling the electrophoresis of rigid polyions: inclusion of ion relaxation. *Macromolecules.* 29:7391–7401.

Allison, S. A. 1998. The primary electroviscous effect of rigid polyions of arbitrary shape and charge distribution. *Macromolecules.* 31: 4464–4474.

Allison, S. A. 1999. Low Reynolds number transport properties of axisymmetric particles employing stick and slip boundary conditions. *Macromolecules.* 32:5304–5312; 7710.

Allison, S. A., and S. Mazur. 1998. Modeling the free solution electrophoretic mobility of short DNA fragments. *Biopolymers.* 46:359–373.

Allison, S. A., and D. Stigter. 2000. A commentary on the screened-Oseen, counterion-condensation formalism of polyion electrophoresis. *Biophys. J.* 78:121–124.

Allison, S. A., and V. T. Tran. 1995. Modeling the electrophoresis of rigid polyions: application to lysozyme. *Biophys. J.* 68:2261–2270.

Allison, S. A., H. Wang, T. M. Laue, T. J. Wilson, and J. O. Wooll. 1999. Visualizing ion relaxation in the transport of short DNA fragments. *Biophys. J.* 76:2488–2501.

Antosiewicz, J., J. M. Briggs, A. H. Elcock, M. K. Gilson, and J. A. McCammon. 1996. Computing ionization states of proteins with a detailed charge model. *J. Comp. Chem.* 17:1633–1644.

Biddle, D., C. Walldal, and S. Wall. 1996. Characterisation of colloidal silica particles with respect to size and shape by means of viscosity and dynamic light scattering measurements. *Colloids Surf.* 118:89–95.

Booth, F. 1954. Sedimentation potential and velocity of solid spherical particles. *J. Chem. Phys.* 22:1956–1968.

CRC Handbook of Chemistry and Physics. 1993. 74th Edition, D. R. Linde, editor. CRC Press, Boca Raton, FL.

Calladine, C. R., C. M. Collis, H. R. Drew, and M. R. Mott. 1991. A study of electrophoretic mobility of DNA in agarose and polyacrylamide gels. *J. Mol. Biol.* 221:981–1005.

Eimer, W., J. R. Williamson, S. G. Boxer, and R. Pecora. 1990. Characterization of the overall and internal dynamics of short oligonucleotides by depolarized dynamic light scattering and NMR relaxation measurements. *Biochemistry.* 29:799–811.

Garcia Bernal, J. M., and J. Garcia de la Torre. 1980. Transport properties and hydrodynamic centers of rigid macromolecules with arbitrary shapes. *Biopolymers.* 19:751–766.

Garcia de la Torre, J., and V. A. Bloomfield. 1981. Hydrodynamic properties of complex, rigid, biological macromolecules: theory and applications. *Quart. Rev. Biophys.* 14:1–139.

Garcia de la Torre, J., A. Jimenez, and J. J. Freire. 1982. Monte Carlo calculation of hydrodynamic properties of freely jointed, freely rotating, and real polymethylene chains. *Macromolecules.* 15:148–154.

Gorti, S., L. Plank, and B. R. Ware. 1984. Determination of electrolyte friction from measurements of the tracer diffusion coefficients, mutual diffusion coefficients, and electrophoretic mobilities of charged spheres. *J. Chem. Phys.* 81:909–914.

Geigenmuller, U. 1984. Commentary on electrolyte friction. *Chem. Phys. Lett.* 110:666–667.

Gurriere, S., S. B. Smith, and C. Bustamante. 1999. Trapping of megabase-sized DNA molecules during agarose gel electrophoresis. *Proc. Natl. Acad. Sci. U.S.A.* 96:453–458.

Hagerman, P. J., and B. H. Zimm. 1981. Monte Carlo approach to the analysis of the rotational diffusion of wormlike chains. *Biopolymers.* 20:1481–1502.

Happel, J., and H. Brenner. 1983. Low Reynolds Number Hydrodynamics. Chap. 5. Martinus Nijhoff, The Hague, The Netherlands.

Henry, D. C. 1931. The cataphoresis of suspended particles. Part I. The equation of cataphoresis. *Proc. R. Soc. London Ser. A.* 203:106–129.

Hoagland, D. A., E. Arvanitidou, and C. Welch. 1999. Capillary electrophoresis measurements of the free solution mobility for several model polyelectrolyte systems. *Macromolecules.* 32:6180–6190.

Huckel, E. 1924. Die kataphorese der kugel. *Physik. Zeitsch.* 25:204–210.

Hunter, R. J. 1981. Zeta potential in Colloid Science. Academic Press, New York.

Klein, S. D., and R. G. Bates. 1980. Conductance of Tris (hydroxymethyl)-aminomethane hydrochloride (Tris-HCl) in water at 25 and 37°C. *J. Sol. Chem.* 9:289–292.

Laue, T. M., T. M. Ridgeway, J. O. Wooll, H. K. Shepard, T. P. Moody, T. J. Wilson, J. B. Chaires, and D. A. Stevenson. 1996. Insights into a new analytical electrophoresis apparatus. *J. Pharm. Sci.* 85:1331–1335.

Jiang, L., D. Yang, and S. B. Chen. 2001. Electroviscous effects of dilute sodium poly(styrenesulfonate) solutions in simple shear flow. *Macromolecules.* 34:3730–3735.

Mazur, S., C. Chen, and S. A. Allison. 2001. Modeling the electrophoresis of short duplex DNA. Counterions K^+ and $Tris^+$. *J. Phys. Chem. B.* 105:1100–1108.

Nuutero, S., B. S. Fujimoto, P. F. Flynn, B. R. Reid, N. S. Ribeiro, and J. M. Schurr. 1994. The amplitude of local angular motion of purines in DNA in solution. *Biopolymers.* 34:463–480.

O'Brien, R. W., and L. R. White. 1978. Electrophoretic mobility of a spherical colloid particle. *J. Chem. Soc. Faraday Trans. 2.* 74: 1607–1626.

Olmstead, M. C., C. F. Anderson, and M. T. Record. 1989. Monte Carlo description of oligoelectrolyte properties of DNA oligomers: range of the end effect and the approach of molecular and thermodynamic properties to the polyelectrolyte limits. *Proc. Natl. Acad. Sci. U.S.A.* 86: 7766–7770.

Overbeek, J. T. G. 1943. Theorie der elektrophorese. Der relaxationseffekt. *Kolloid-Beih.* 54:287–364.

Rasmusson, M., and B. Akerman. 1998. Dynamic mobility of DNA. *Langmuir.* 14:3512–3516.

Rizzo, V., and J. A. Schellman. 1981. Flow dichroism of T7 DNA as a function of salt concentration. *Biopolymers.* 20:2143–2163.

Ross, P. D., and R. L. Scruggs. 1964. Electrophoresis of DNA. III. The effect of several univalent electrolytes on the mobility of DNA. *Biopolymers.* 2:231–236.

Rouzina, I., and V. A. Bloomfield. 1996. Competitive electrostatic binding of charged ligands to polyelectrolytes: planar and cylindrical geometries. *J. Phys. Chem.* 100:4292–4304.

Schellman, J. A., and D. Stigter. 1977. Electrical double layer, zeta potential, and electrophoretic charge of double-stranded DNA. *Biopolymers.* 16:1415–1434.

Schurr, J. M. 1980. A theory of electrolyte friction of translating polyelectrolytes. *Chem. Phys.* 45:119–132.

Schurr, J. M. 1984. Reply to comment on electrolyte friction. *Chem. Phys. Lett.* 110:668–670.

Schurr, J. M., and S. B. Smith. 1990. Theory for the extension of a linear polyelectrolyte attached at one end in an electric field. *Biopolymers.* 29:1161–1165.

Sherwood, J. D. 1980. The primary electroviscous effect in a suspension of spheres. *J. Fluid Mech.* 111:347–366.

Smith, S. B., and A. J. Bendich. 1990. Electrophoretic charge density and persistence length of DNA as measured by fluorescence microscopy. *Biopolymers.* 29:1167–1173.

Smoluchowski, M. 1921. Elektrische endosmose und stromungsstrome. *In* Handbuch del Elektrizitat und des Magnetismus Volume 2. L. Graetz, editor. Barth, Leipzig, Germany.

Stellwagen, N. C., C. Gelfi, and P. G. Righetti. 1997. The free solution mobility of DNA. *Biopolymers.* 42:687–703.

Stellwagen, N. C., C. Gelfi, and P. G. Righetti. 1999. DNA-histidine complex formation in isoelectric histidine buffers. *J. Chromat. A.* 838: 179–189.

Stellwagen, N. C., C. Gelfi, and P. G. Righetti. 2000. DNA and buffers: the hidden danger of complex formation. *Biopolymers.* 54:137–142.

Stigter, D. 1975. The charged colloidal cylinder with a Gouy double layer. *J. Coll. Interface Sci.* 53:296–306.

Stigter, D. 1978a. Electrophoresis of highly charged colloidal cylinders in univalent salt solutions. 1. Mobility in transverse field. *J. Phys. Chem.* 82:1417–1423.

Stigter, D. 1978b. Electrophoresis of highly charged colloidal cylinders in univalent salt solutions. 2. Random orientation in external field and application to polyelectrolytes. *J. Phys. Chem.* 82:1424–1429.

Stigter, D. 1982a. Primary charge effect on the sedimentation of long, colloidal rods. *J. Phys. Chem.* 86:3553–3558.

Stigter, D. 1982b. Mobility of water near charged interfaces. *Adv. Coll. Interface Sci.* 16:253–265.

Stigter, D. 1991. Shielding effects of small ions in gel electrophoresis of DNA. *Biopolymers.* 31:169–176.

Stigter, D. 2000. A novel interpretation of steady-state electrophoresis experiments. *J. Phys. Chem. B.* 104:3402–3406.

Stigter, D., and C. Bustamante. 1998. Theory for the hydrodynamic and electrophoretic stretch of tethered B-DNA. *Biophys. J.* 75:1197–1210.

Tirado, M. M., and J. Garcia de la Torre. 1979. Translational friction coefficients of rigid, symmetric top macromolecules. Application to circular cylinders. *J. Chem. Phys.* 71:2581–2587.

Tirado, M. M., C. L. Martinez, and J. Garcia de la Torre. 1984. Comparison of theories for the translational and rotational diffusion coefficients of rod-like macromolecules. Application to short DNA fragments. *J. Chem. Phys.* 81:2047–2052.

Vizcarra-Rendon, A., M. Medina-Noyola, and R. Klein. 1990. Electrolyte friction on non-spherical polyions. *Chem. Phys. Lett.* 173:397–402.